Selective internalization of self-assembled artificial oil bodies by HER2/*neu*-positive cells

2011 Nanotechnology 22 015102

(http://iopscience.iop.org/0957-4484/22/1/015102)

Nanotechnology **22** (2011) 015102 (11pp) doi:10.1088/0957-4484/22/1/015102

Selective internalization of self-assembled artificial oil bodies by HER2/*neu*-positive cells

Chung-Jen Chiang[1,4], Li-Jen Lin[2], Che-Chin Lin[1], Chih-Hsiang Chang[3] and Yun-Peng Chao[3,4]

[1] Department of Medical Laboratory Science and Biotechnology, China Medical University, Taichung, Taiwan
[2] School of Chinese Medicine, China Medical University, Taichung, Taiwan
[3] Department of Chemical Engineering, Feng Chia University, Taichung, Taiwan

E-mail: cjchiang@mail.cmu.edu.tw and ypchao@fcu.edu.tw

Received 7 September 2010, in final form 20 October 2010
Published 6 December 2010
Online at stacks.iop.org/Nano/22/015102

Abstract

A novel delivery carrier was developed using artificial oil bodies (AOBs). Plant seed oil bodies (OBs) consist of a triacylglycerol matrix surrounded by a monolayer of phospholipids embedded with the storage protein oleosin (Ole). Ole consists of a central hydrophobic domain with two amphiphatic arms that extrude from the surface of OBs. In this study, a bivalent anti-HER2/*neu* affibody domain (ZH2) was fused with Ole at the C terminus. After overproduction in *Escherichia coli*, the fusion protein (Ole-ZH2) was recovered to assemble AOBs. The size of self-assembled AOBs was tailored by varying the oil/Ole-ZH2 ratio and pH to reach a nanoscale. Upon co-incubation with tumor cells, the nanoscale AOBs encapsulated with a hydrophobic fluorescence dye were selectively internalized by HER2/*neu*-overexpressing cells and displayed biocompatibility with the cells. In addition, the ZH2-mediated endosomal entry of AOBs occurred in a time- and AOB dose-dependent manner. The internalization efficiency was as high as 90%. The internalized AOBs disintegrated at the non-permissive pH (e.g. in acidic endosomes) and the cargo dye was released. Results of *in vitro* study revealed a sustained and prolonged release profile. Taken together, our findings indicate the potential of AOBs as a delivery carrier.

1. Introduction

Cancer is the most life-threatening disease in humans. One promising treatment of this disease involves the delivery of chemotherapeutic drugs to cancerous sites without damaging normal cells. This approach, commonly recognized as targeted cancer therapy, requires the selective association of a target ligand with a tumor cell-specific biomarker. One well-known paradigm is the treatment of metastatic breast cancer with the humanized antibody trastuzumab (Herceptin®). Through the interaction with human epidermal growth factor receptor 2 (HER2/*neu*), trastuzumab is capable of inducing many cytotoxic effects in a direct or indirect manner [1]. However, these antibody-dependent cytotoxic actions are usually insufficient [2]. Owing to the large sizes of monoclonal antibodies, antibody mimetics with much smaller sizes have been proposed as a potential alternative [3].

Many potent anti-cancer pharmaceuticals are poorly soluble, making targeted delivery of these hydrophobic agents via oral or intravenous administration challenging. The common problem encountered with the administration of these water-repelling drugs is that it leads to low bioavailability and high local concentration of drugs at the site of the aggregate deposition [4, 5]. To address this issue, various drug delivery systems have been developed on a nanoscale, such as liposomes [6], synthetic polymers [7], micelles [8], and many others [9]. Although some promising results have been reported, many technical difficulties need to be overcome [10]. In addition, a reduction in undesirable side effects caused by drug toxicity is equally important. Therefore, it is imperative

[4] Authors to whom any correspondence should be addressed.

that a drug carrier with superior tumor-targeting ability be developed.

Plant seeds store triacylglycerols (TAGs) in discrete intracellular organelles, called oil bodies (OBs), and use them as fuel for germination and subsequent seedling growth [11, 12]. OBs contain a TAG matrix that is surrounded by a monolayer of phospholipids (PLs) embedded with storage proteins [13]. It is generally recognized that OBs are endogenously encapsulated with the aid of storage proteins such as oleosin (Ole) [14]. Ole comprises a lipophilic core that is embedded into OBs and two hydrophilic domains at the N and C terminus that protrude outward [15]. In addition, Ole provides steric hindrance and electronegative repulsion, thereby contributing to the substantial stability of OBs both in cells and in isolated preparations [16, 17]. This remarkable feature has made OBs very attractive for biotechnological applications.

Artificial OBs (AOBs) have been successfully created by self-assembly of biomaterials consisting of plant oils, PLs, and Ole [18]. The size of AOBs can be tailored by varying the ratio of the matrix oil to Ole. In particular, AOBs prepared from the recombinant Ole expressed in *Escherichia coli* are comparable in size, topology, and stability to OBs encapsulated with native Ole derived from plant seeds [16, 18]. The practicality of preparing AOBs has ushered in many useful applications, including a bacterial expression/purification system for producing recombinant proteins [19, 20], encapsulation of probiotics for oral administration [21], and enzyme immobilization [22]. Given that they are small, stable, biocompatible, and biodegradable, AOBs (mainly comprising natural lipids) with hydrophobic cores have the potential as a delivery carrier. In this study, we present data showing that AOBs could be shaped to reach nanoscale size and to display an anti-HER2/*neu* motif on their surface. This was approached by fusing a bivalent anti-HER2 affibody (denoted as ZH2) to Ole [23]. After overproduction in *E. coli*, this fusion protein (Ole-ZH2) was recovered to assemble AOBs with entrapment of a hydrophobic fluorescence dye. Upon co-incubation with tumor cells, these engineered AOBs were able to target and penetrate cells overexpressing HER2/*neu*. Consequently, disruption of internalized AOBs was triggered in response to acidic pH and the cargo dye was released.

2. Experimental method

2.1. DNA manipulation

Using polymerase chain reaction (PCR), the DNA fragment containing ZH2 was amplified from plasmid pDW-ZH2 (Y P Chao) using two primers, JO0805 (ACAACCCATGGA-GATATCGGAATTAATTC) and RC07143 (CCAAGAAGC-TTT-TTCGGCGCCTG). The resulting DNA was ligated into the *Sma*I-trimmed pBluescriptII-SK (Stratagene) to give plasmid pBlue-ZH2. After recovering the ZH2-carrying fragment from pBlue-ZH2 by *Nco* I-*Hind* III cleavage, the fragment was incorporated into the corresponding sites of plasmid pJO1-Ole [20] to produce plasmid pJO1-Ole-ZH2. Consequently, plasmid pJO1-Ole-ZH2 contained the N-terminal fusion of Ole with ZH2 under the control of the T7 promoter. Plasmid pJO1-Ole carrying Ole alone was used as the control.

2.2. Bacteria culturing and protein analysis

The plasmids pJO1-Ole-ZH2 and pJO1-Ole were transformed into *E. coli* strain BL21(DE3) to obtain recombinant bacteria, BL21(DE3)/pJO1-Ole-ZH2 and BL21(ED3)/pJO1-Ole. For protein production, recombinant bacteria were cultured in shake flasks containing Luria–Bertani (LB) medium [24] overnight. After the seeding of the overnight culture into fresh LB medium, bacterial cultures were maintained at 37 °C and monitored for growth by turbidimetrical measurement at 550 nm (OD_{550}) along the time course. Upon reaching a cell density of 0.5 at OD_{550}, the bacterial culture was induced with 100 μM IPTG for protein production. Bacteria were harvested 4 h later by centrifugation and resuspended in 1 ml of 10 mM sodium phosphate buffer (PBS) at pH 7.5. After disruption of bacteria by sonication, centrifugation was applied to separate the supernatant and the pellet. As reported previously [25], proteins were analyzed by sulfate-polyacrylamide gel electrophoresis (SDS-PAGE). Following electrophoresis, the gel was stained with Coomassion blue R-250. The relative levels of recombinant proteins produced were quantified using the Image Analyzer GAS9000 (UVItech, England).

2.3. Immunoassay

For immunoassay, proteins in the SDS-PAGE gel were blotted onto a nitrocellulose membrane using a Bio-Rad Trans-Blot system (Bio-Rad) according to the manufacturer's instructions. The membrane was subjected to immunodetection with 1:200 diluted mouse anti-6xHis monoclonal antibody (Genemark Technology Co. Ltd, Taiwan) at room temperature for 1 h. The membrane was washed in PBS and then exposed to a 200-fold dilution of FITC-conjugated anti-mouse IgG (Jackson Immuno Research, USA) for 1 h. The reaction was incubated with 3 mM 4-chloro-1-naphthol containing 0.015% H_2O_2 for color development. Alternatively, AOBs were fixed in 2.5% (w/v) paraformaldehyde. After washing with PBS, AOBs were blocked by immersing in a solution consisting of 3% BSA in PBS at room temperature for 1 h. Immunodetection of AOBs against the anti-6xHis antibody was carried out in a similar manner. AOBs were then mounted on glass slides for observation by fluorescence microscopy (Olympus IX71, Japan).

2.4. Self-assembly of AOBs

AOBs were assembled as previously reported with minor modifications [20]. At the end of culturing, bacteria were harvested and resuspended in 1 ml PBS to reach a cell density of 10 at OD_{550}. Following disruption by a French press, centrifugation was applied and the supernatant and pellet were fractioned. Unless stated otherwise, AOBs were constituted of 1 ml PBS with 100 μg of sesame oil, 150 μg of PL, and 100 μg of purified Ole or Ole-ZH2 fusion protein at

pH 7.5 and 4 °C. Fluorescent AOBs were formed in the same way except that 1 μg yellow GGK dye (Widetex Co., Taiwan) was added. The plant oils utilized included soybean oil (Taiwan Sugar Co., Taiwan), peanut oil (Leader Price Co., Taiwan), sesame oil (Taisun Co., Taiwan), olive oil (Taisun Co., Taiwan), and mineral oil (Sigma, MO). The mixture was subjected to sonication with the amplitude set at 20% for 10 s; this was repeated three times on ice. Subsequently, AOBs were collected after centrifugation and washed with the buffer solution.

2.5. Morphology, size, and stability of AOBs

The morphology of AOBs prepared in various conditions was analyzed by a light microscope (Nikon type E600, Japan), as described previously [18]. The size of AOBs was determined by measurement of light scattering at a 90° angle with an N4-submicron particle size analyzer (Beckman Coulter, USA). AOBs were also analyzed using transmission electron microscopy (TEM) (Jeol JEM-1400, Japan). One drop of ZH2-displayed AOB suspension was placed on a 400 mesh copper grid coated with carbon. After deposition for 2 min, the grid was blotted with filter paper to remove surface water before negative staining with uranyl acetate solution. The stability of AOBs was determined by the turbidity test as reported previously [18]. In brief, 1 ml AOBs solution was placed in a cuvette, covered with parafilm, and kept at the indicated condition. The absorbance (A) of the suspension in the lower portion of the cuvette was measured at 600 nm with a spectrophotometer (Beckmen DU 530, USA). The absorbance obtained at the beginning (A_0) and time intervals (A) was used to calculate the relative turbidity.

2.6. Tumor cell culture

Human cancer cell lines, MDA-MB-231 (ovarian), SKOV3 (ovarian), MCF7 (breast) and MCF7/Her18 (HER2-transfected stable cell line), were grown on McCoy's 5A and Dulbecco's modified Eagle's medium/F12 medium (HyClone Lab., USA) supplemented with 10% fetal bovine serum (FBS), 2% L-glutamine, 1% penicillin, and 1% streptomycin. These cells were cultured at 37 °C in a humidified atmosphere of 5% in the presence of CO_2. The culture medium was changed every two days until cell confluence reached 80%. Cell concentration was calculated using a hemocytometer, and cells were resuspended and seeded into a 24-well plate to reach 1×10^5 cells/well.

2.7. Assessment of cytotoxicity

The biocompatibility of AOBs with cell lines was examined using a cell-counting kit (Dojindo Molecular Technologies, Inc.). SKOV3 and MDA-MB-231 cancer cells were cultured in a 96-well plate at an initial seeding density of 5×10^3 cells per well. After 24 h, the growth medium was removed and replaced with fresh medium without serum and phenol red. Subsequently, various amounts of free dye or dye-loaded AOBs were added. After incubation for 24, 48, and 72 h, cells were washed with PBS and cultured in DMEM with 10% WST-8 solution for another 2 h. The absorbance of each well was measured at 450 nm with a microplate reader (SpectraMax M2, Molecular Device, USA). Cell viability was calculated as the ratio of absorbance of AOB-treated cells relative to untreated cells. All experiments were performed three times.

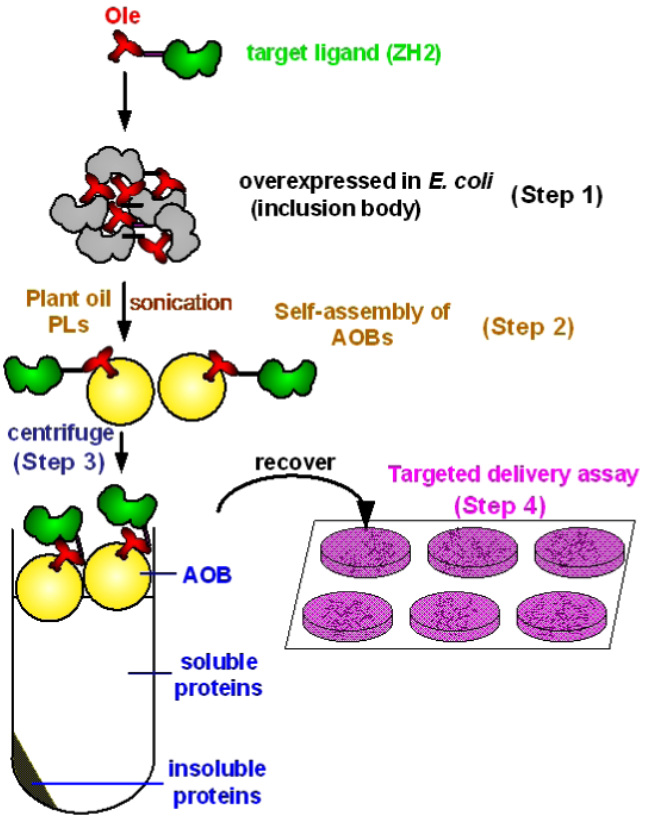

Figure 1. The general procedure for preparing self-assembled AOBs. In the first step, Ole was fused with the ligand of interest (e.g. ZH2) and overexpressed in *E. coli*. Second, AOBs were assembled by subjecting a mixture consisting of TAG (plant oil), PLs, and the fusion protein (e.g. Ole-ZH2) to sonication. To encapsulate the cargo, the cargo agent was added to the mixture before self-assembly of AOBs. Third, AOBs were recovered from the top of the solution after centrifugation. Finally, the targeted delivery assay was carried out with AOBs.

(This figure is in colour only in the electronic version)

2.8. In vitro study of dye release

The release profiles of Yellow GGK from AOBs were measured using a dialysis bag with a molecular weight cut-off ranging from 12 000 to 14 000 (Spectrum Laboratories, USA), as described previously [20]. The buffer medium comprised 20 ml of 0.01 M PBS at pH 7.5 or pH 6.5. AOBs of 1 ml were placed in a dialysis bag and immersed in the medium at 37 °C under constant stirring. At time intervals, 100 μl aliquots of the medium were withdrawn and replenished by adding an equal volume of PBS. The content of dye (Yellow GGK) in the withdrawn PBS was measured by a spectrofluorometer (FP-6200, Jasco, Japan). The absorbance was normalized to that of the initial dye content. All experiments were performed in triplicate.

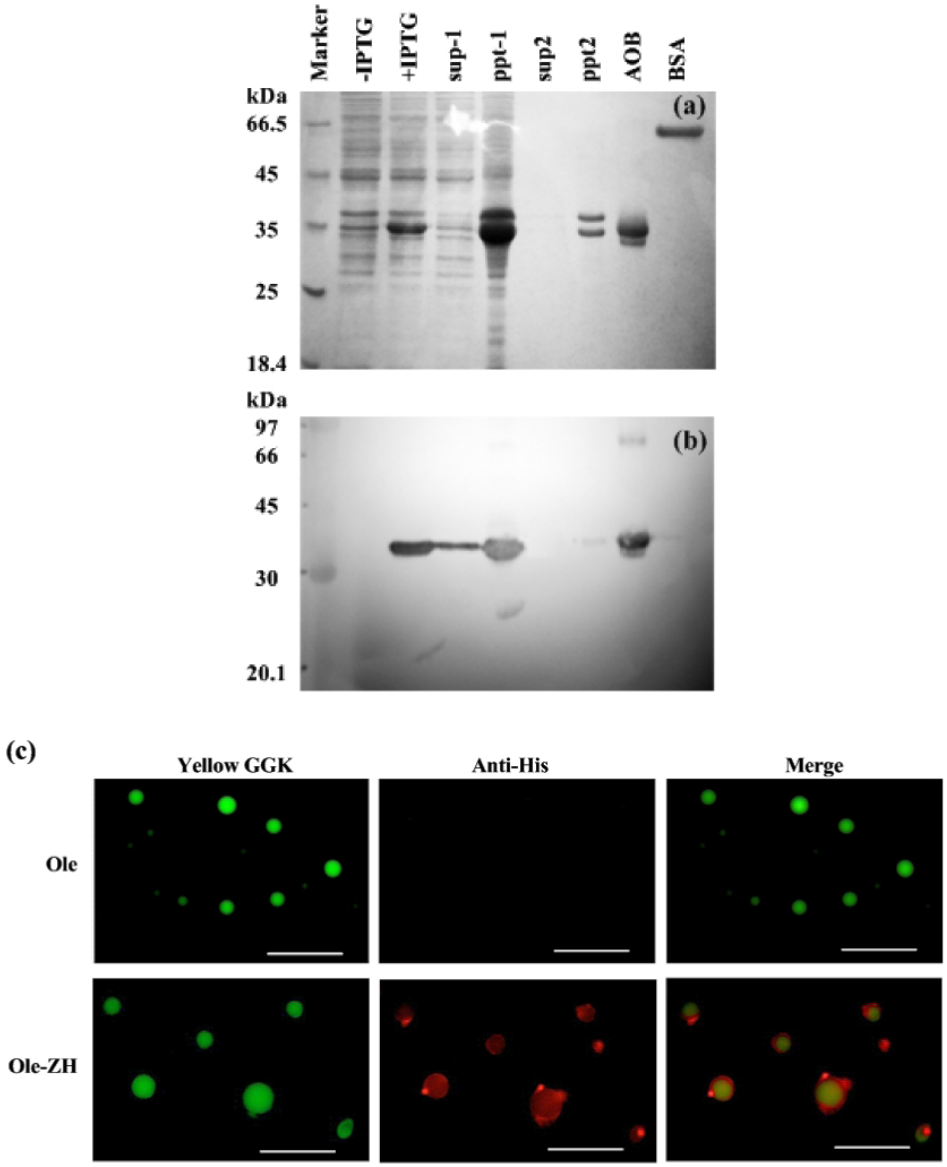

Figure 2. Analysis of ZH2-displayed AOBs. (a) Recombinant *E. coli* strains were cultured and induced by IPTG for protein production. Total proteins from induced (+IPTG) and uninduced (−IPTG) strain BL21(DE3)/pJO1-Ole-ZH2 were resolved in SDS-PAGE. In addition, the total protein of strain BL21(DE3)/pJO1-Ole-ZH2 was fractioned into soluble (sup-1) and insoluble (ppt-1) parts. Ole-ZH2 from ppt-1 was recovered to assemble AOBs by sonication. After centrifugation, the AOBs were separated from the supernatant (sup-2) and precipitate (ppt-2). AOBs were isolated and heated to release the incorporated protein (AOB). (b) The SDS-PAGE was blotted onto a nitrocellulose membrane and an immunoassay was conducted using the anti-6xHis tag antibody. (c) Encapsulated with a hydrophobic dye (green), AOBs composed of Ole or Ole-ZH2 were against the anti-6xHis tag antibody (red). The immunodetection was observed with fluorescence microscopy. The scale bar equals 2 μm.

2.9. Microscopy and flow cytometry

Tumor cells were washed with PBS and incubated with fluorescent AOBs for various times at 37 °C. Subsequently, cells were washed with PBS containing 0.01% Tween-20 once and PBS twice to remove unbound AOBs. A blocking solution consisting of 3% FBS albumin in PBS was added to cells at room temperature for 1 h. Finally, a 200-fold dilution of anti-HER2/*neu* antibody (Santa Cruz Biotech., USA) was added and allowed to react at room temperature for 1 h. After rinsing three times with PBS, a 500-fold dilution of anti-mouse IgG-TRIAC (Jackson ImmunoResearch Lab., USA) was added, allowed to react, and then washed with PBS to remove the unbound secondary antibody. In addition, cell nuclei were stained with a 15 000-fold dilution of diamidino-2-phenylindole (DAPI) and washed with PBS. The cells were visualized with a fluorescence microscope (Olympus IX71, Japan) and confocal microscopy (Leica TCS SP2, Germany).

Alternatively, tumor cells were seeded into a 6-well plate (1×10^5 cells/well) and grown to 80% confluence. After incubation with AOBs, cells were washed twice with PBS. Following trypsinization, cells were harvested by centrifugation and resuspended in PBS. Analysis of internalized AOBs was conducted using a FACScanto flow cytometer system (Becton Dickinson, USA). All experiments were performed in triplicate.

3. Results and discussion

3.1. Protein production and self-assembly of ZH2-based AOBs

This preliminary study was to explore the potential of AOBs as a delivery carrier. We first chose to target HER2/*neu* in tumor cells. HER2/*neu* belongs to the human epidermal growth factor receptor family [26], and abnormal overexpression of HER2/*neu* can lead to the progression of aggressive tumors [27]. Antibody mimetics of small size were selected because of their ability to interact with HER2/*neu*. This is based on the fact that monoclonal antibodies of large size are easily taken up by the liver and exhibit slow blood clearance as well as poor tissue penetration [28]. Among various biomimetics, affibodies are of particular interest. They are derived from one of the IgG-binding domains of staphylococcal protein A and comprise only 58 amino acid residues. Extensive screening of a phage display library revealed that the anti-HER2/*neu* affibody (Z-HER2:342 affibody) has very high binding affinity ($k_D \sim 22$ pM) to the extracellular domain of HER2/*neu* [23].

To target HER2/*neu*-positive cells, AOBs were modified to display the anti-HER2 affibody. This was done by fusing of Ole with ZH2, and the resulting fusion protein was overexpressed in bacterial strain BL21(DE3)/pJO1-Ole-ZH2. The control strain BL21(ED3)/pJO1-Ole was cultured in a similar fashion. Self-formation of AOBs was carried out following the general procedure outlined in figure 1. As shown in figure 2(a), the fusion protein was overexpressed in strain BL21(DE3)/pJO1-Ole-ZH2 upon IPTG induction and was mainly present in the insoluble fraction of cell lysate (ppt-1). Ole-ZH2 was then isolated from ppt-1 and employed for self-assembly of AOBs. After centrifugation, AOBs floated on the top of the supernatant (sup-2) and little Ole-ZH2 was left in the cell pellet (ppt-2). Finally, AOBs were subjected to heating to liberate the incorporated proteins. Ole-ZH2 was identified as the main protein. The result indicates the strong association of Ole-ZH2 with plant oil and PLs. As a control, Ole in the insoluble form could also be overproduced in strain BL21(ED3)/pJO1-Ole after induction by IPTG (data not shown).

The construction of plasmid pJO1-Ole-ZH2 resulted in the fusion of a 6xHis tag with Ole-ZH2 at the C terminus. As shown in figure 2(b), this fusion protein could be detected with the anti-6xHis tag antibody. Moreover, the anti-6xHis tag antibody was applied and the fluorescence signal was found surrounding Ole-ZH2-based AOBs (figure 2(c)). In contrast, no fluorescence signal could be observed for Ole-based AOBs. Overall, the result suggests the surface display of the fusion partner via Ole onto AOBs.

3.2. Formation of stable nanoscale AOBs

Various types of plant oils were investigated in an attempt to tailor the size of AOBs. The weight ratio of plant oil to Ole-ZH2 at 1:1 was exploited for assembly of ZH2-based AOBs at 4 °C and pH 7.5. Repeated treatment by sonication led to the formation of stable ZH2-displayed AOBs in all types of oils examined with the exception of mineral and peanut oil

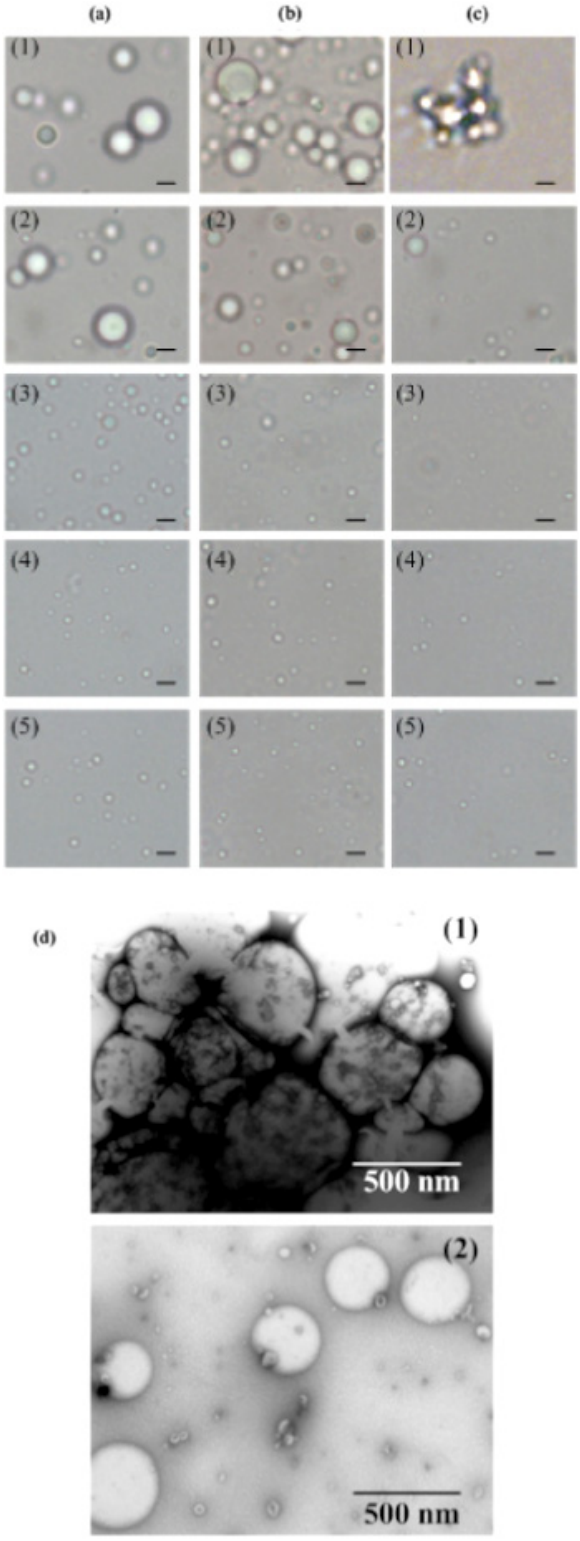

Figure 3. Self-assembly of ZH2-displayed AOBs at various conditions. AOBs were assembled in various conditions and analysed by microcopy. (a) AOBs were assembled with various plant oils, including (1) mineral oil, (2) peanut oil, (3) soybean oil, (4) olive oil, and (5) sesame oil. (b) AOBs were assembled with various weight ratios of sesame oil to Ole-ZH2 at (1) 10:1, (2) 2:1, (3) 1:1, (4) 1:2, and (5) 1:10. (c) AOBs were assembled at pH (1) 6.5, (2) 7.0, (3) 7.5, (4) 8.0, and (5) 9.0. The scale bar equals 2 μm. (d) Micrographs of AOBs at (1) pH 6.5 and (2) 7.5 were taken with a transmission electron microscope (TEM).

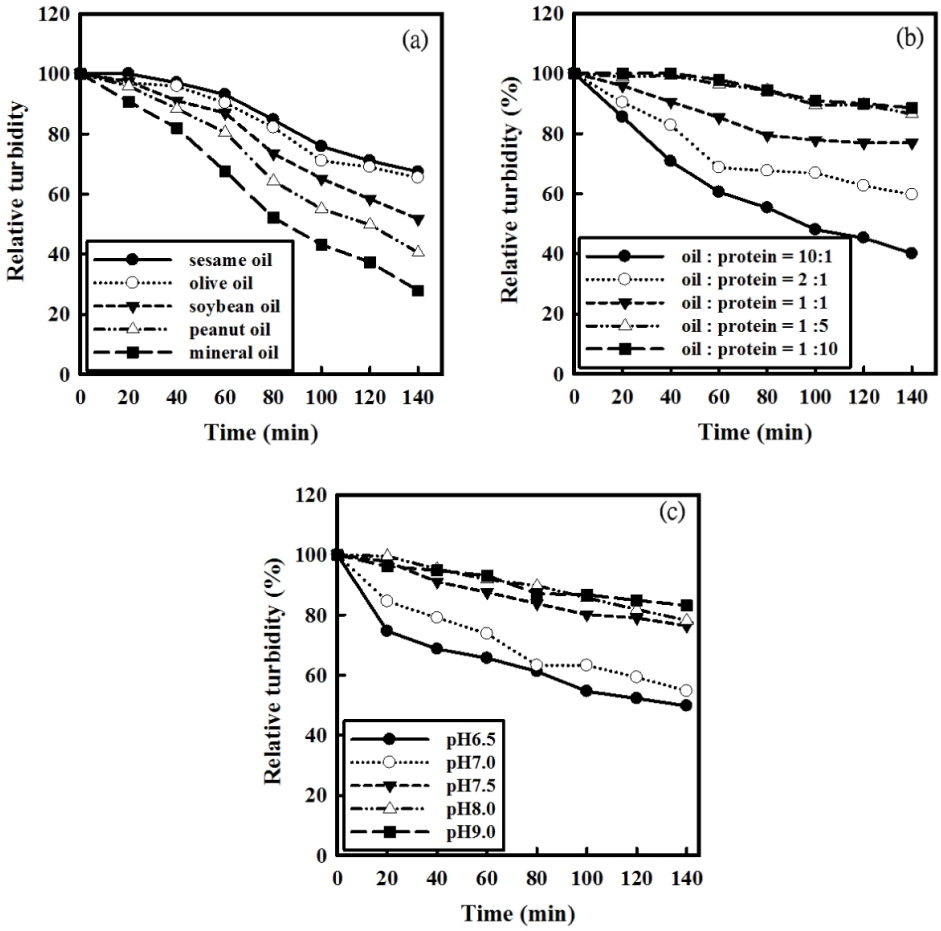

Figure 4. Stability of ZH2-displayed AOBs assembled in various conditions was evaluated as described in section 2. The stability of AOBs assembled in various conditions was examined by the turbidity test as described. (a) AOBs were assembled with various oils. (b) AOBs were assembled with various weight ratios of sesame oil to Ole-ZH2. (c) AOBs were assembled at various pHs.

Table 1. Size of ZH2-based AOBs assembled with various (A) plant oils, and at various (B) oil/Ole-ZH2 ratios, and (C) pHs.

(A)		(B)		(C)	
Oil	Mean particle size (nm)	Oil/Ole-ZH2 (w/w)	Mean particle size (nm)	pH	Mean particle size (nm)
Mineral oil	1264.1 ± 47.7[a]	10:1	1543.8 ± 95.8	6.5	896.5 ± 33.1
Peanut oil	893.5 ± 14.1	2:1	1113.8 ± 24.0	7.0	785.2 ± 30.4
Soybean oil	817.9 ± 14.7	1:1	725.1 ± 29.5	7.5	558.9 ± 37.0
Sesame oil	725.1 ± 29.5	1:5	558.9 ± 37.0	8.0	454.6 ± 21.0
Olive oil	751.0 ± 23.3	1:10	286.1 ± 22.2	9.0	418.3 ± 46.3

[a] Each data point represents the mean ± standard deviation from three independent measurements.

(figure 3(a)). As indicated in table 1, the size of AOBs ranged from 500 to 1250 nm. Stability of AOBs was examined by the turbidity test. Figure 4(a) shows that AOBs made of olive or sesame oil were more stable than those composed of soybean, peanut, or mineral oil. The result may reflect the distinct TAG constitutions of various oils, leading to various degrees of interaction with Ole-ZH2. Accordingly, sesame oil was chosen for further experiments.

Different weight ratios of sesame oil to Ole-ZH2 (oil/protein) were examined at pH 7.5 and 4 °C. As shown in figure 3(b), a higher ratio (e.g. more oil than Ole-ZH2) led to coalescence of AOBs. This was likely due to the weakness of the steric repulsion force provided by Ole. It was found that integral ZH2-based AOBs could be formed at lower oil/protein ratios. In general, the size reduced with the decreasing ratio. The average size of AOBs showed a normal distribution profile, and their sizes were in the range of 280–1550 nm (table 1). Results of the turbidity test revealed that nanoscale AOBs with oil/protein ratios of 1:5 and 1:10 remained relatively stable (figure 4(b)).

Finally, the effect of pH on AOBs assembled with an oil/protein ratio of 1:5 was investigated. As depicted in figure 3(c), ZH2-based AOBs were prone to coalescing at pH values between 6.5 and 7 while remaining as individually

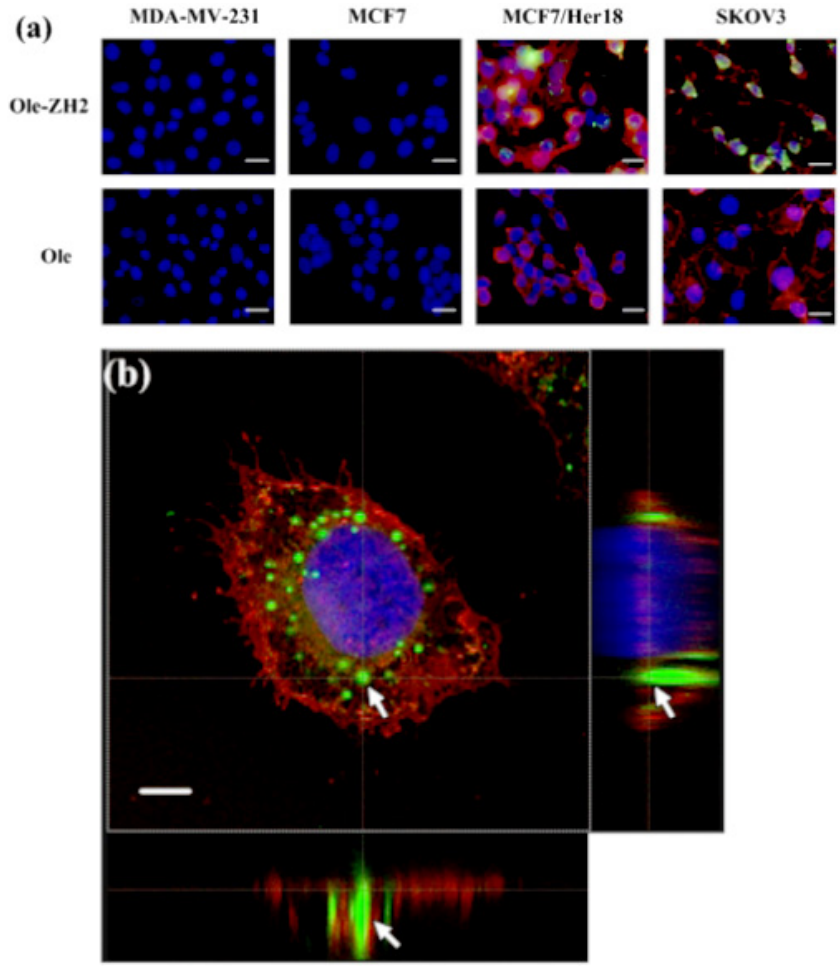

Figure 5. Selective internalization of ZH2-displayed AOBs into tumor cells. AOBs, composed of Ole-ZH2 or Ole, were assembled to encapsulate 1 μg ml^{-1} yellow GGK dye. Subsequently, fluorescent AOBs (green) were resuspended in PBS and added to 1×10^5 cells to reach a final concentration of 25 μg ml^{-1} for 2 h. After washing with PBS three times, treated cells were processed for analyses. (a) For observation by fluorescence microscopy, cell nuclei (blue) and the HER2/*neu* receptor (red) were stained with DAPI and anti-HER2/*neu* antibody, respectively. The images were individually captured and then merged. The scale bar equals 20 μm. (b) AOB-treated MCF7/Her18 cells were further analyzed by confocal laser scanning microscopy (CLSM). The panel represents a section taken from the stack on the z axis. The insets representing two three-dimensional reconstruction sections, perpendicular or parallel to the monolayer plane, are shown below (x–z section) and to the right (y–z section).

discrete particles at pH values higher than pH 7.5. Indeed, AOBs exhibit instability in acidic conditions [18, 20]. This was further confirmed by observation with TEM (figure 3(d)). It is likely that the electronegative repulsion force provided by Ole in AOBs is diminished in acidic conditions. AOBs, therefore, undergo coalescence and disintegration. In addition, the size of these integral AOBs was found in the range of 420–550 nm (table 1). They were also highly stable along the time course (figure 4(c)).

3.3. Selective internalization of ZH2-displayed AOBs

Our next task was to see whether AOBs equipped with ZH2 were functional. Therefore, AOBs were entrapped with a hydrophobic fluorescent dye and assembled in the following conditions: sesame oil/protein ratio of 1:5 and pH 7.5. As a consequence, the size of AOBs ranged from 420 to 500 nm, and their stability remained unaffected when 1 μg ml^{-1} fluorescent dye was encapsulated. Subsequently, the resulting fluorescent AOBs with ZH2 were co-incubated with tumor cells. As shown in figure 5(a), strong fluorescence signals were captured in HER2/*neu*-overexpressing cells (e.g. MCF7/Her18 and SKOV3) whereas the signal was absent in the HER2/*neu*-negative cells (e.g. MCF7 and MDA-MB-231). In contrast, no signals were detected in any of the cells exposed to ZH2-free AOBs (e.g. assembled from Ole). The result implies that the ZH2 motif via Ole was correctly presented on the AOB surface, which in turn results in the association of AOBs with HER2/*neu*-positive cells.

To further confirm the localization of AOBs, z-axis scanning fluorescence microscopy and 3D image reconstitution were utilized. The result showed that ZH2-displayed AOBs were located in the cytoplasm of HER2/*neu*-overexpressing cells (figure 5(b)). Overall, the above-mentioned results imply that ZH2-displayed AOBs were selectively internalized by HER2/*neu*-positive cells.

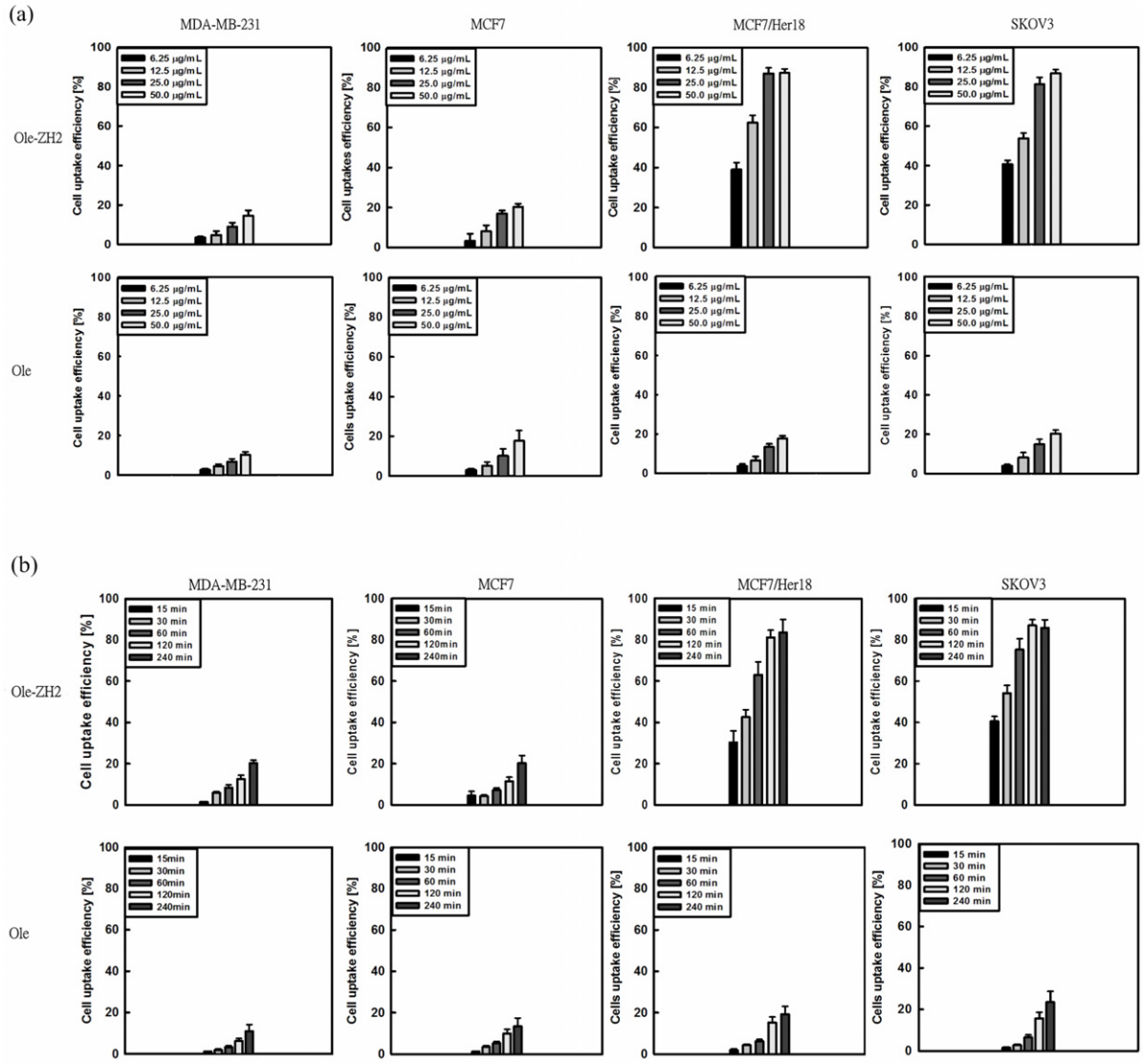

Figure 6. Internalization efficiency of AOBs into tumor cells was assessed by flow cytometry and fluorescence microscopy. Fluorescent AOBs (green) were incubated with tumor cells for further analyses. (a) After co-incubation with various concentrations of AOBs for 2 h, cells were processed for analysis by flow cytometry. (b) The effect of incubation time was investigated by flow cytometry. All experiments were conducted in triplicate. The cell lines used for analyses are indicated on the top of each panel. Symbols: Ole-ZH2, Ole-ZH2-based AOBs; Ole, Ole-based AOBs. (c) Cells treated with various doses of AOBs were analyzed by fluorescence microscopy. The AOB doses are shown on the left of each panel. (d) Cells treated with AOBs for various times were analyzed by fluorescence microscopy. The incubation time is shown on the left of each panel.

3.4. Internalization efficiency of ZH2-displayed AOBs

The internalization efficiency of HER2/*neu*-positive cells was calculated as the percentage of fluorescence-emitting cells in the entire cell population. First, various doses of AOBs were co-incubated with tumor cells for 2 h. Cells were then collected and processed for analysis by flow cytometry. As shown in figure 6(a), the percentage of cells emitting green fluorescence increased as the dose of AOB increased. This was also confirmed by fluorescence microscopy (figure 6(c)). The maximal efficiency was obtained at 25 μg ml^{-1} AOBs. At that concentration, the efficiency was greater than 90% for HER2/*neu*-positive cells, MCF17/Her18, and SKOV3.

Tumor cells were also co-incubated with fluorescent AOBs (25 μg ml^{-1}) for various time periods. At the end of incubation, cells were prepared for analysis by flow cytometry. As shown in figure 6(b), the internalization efficiency of ZH2-displayed AOBs correlated positively with the incubation time. A similar observation was obtained with fluorescence microscopy in which the maximal efficiency was reached when the incubation time lasted for 1 h (figure 6(d)). This time-dependent internalization behavior is consistent with the reported invasion kinetics of anti-HER2/*neu* affibody-conjugated materials [29].

3.5. Release of the cargo dye

The translocation path of HER2/*neu* receptor to cell nucleus has been proposed [30]. It starts with endocytic internalization

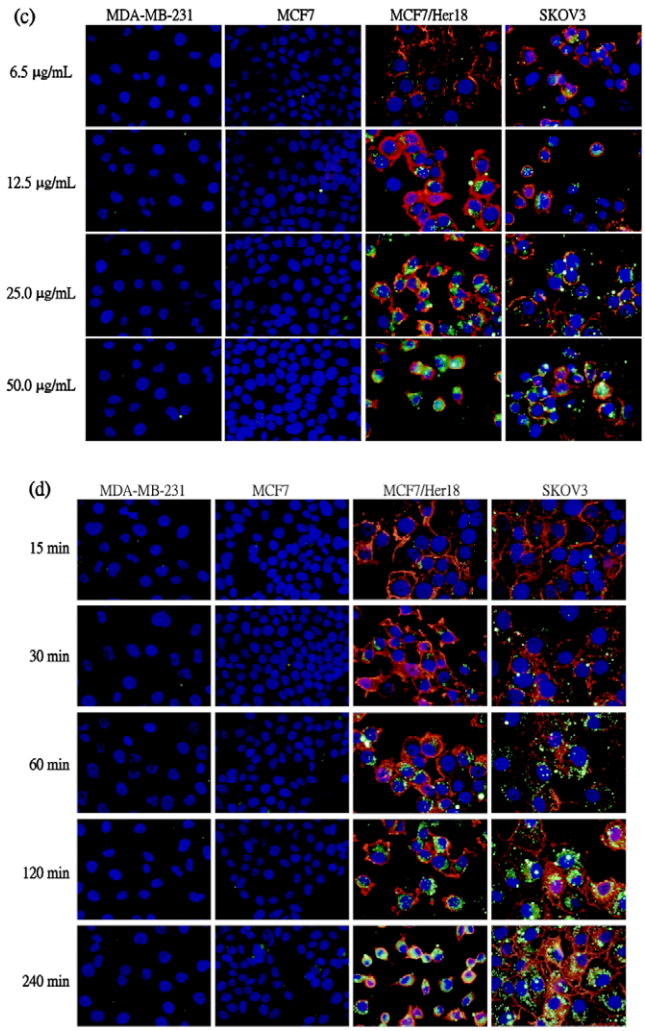

Figure 6. (Continued.)

of the HER2/*neu* receptor. Followed by interaction with the transport receptor called importin, the HER2/*neu* receptor associated with the nuclear pore protein travels to the cell nucleus. Therefore ZH2-displayed AOBs are most likely internalized into cells via the endosomal entry pathway. As indicated in figure 7(a), lysosomes of cells were stained by LysoSensor blue DND-167 after treatment with fluorescent ZH2-displayed AOBs. The result showed that the green fluorescence emitted by AOBs co-localized mostly with the blue fluorescence emitted by LysoSensor, indicating that AOBs were located inside the cell lysosomes.

AOBs tend to coalesce in acidic conditions, ultimately resulting in their disintegration, as illustrated in figure 3(d). This might confer on AOBs a control-and-release feature upon entry into acidic endosomes [31]. To explore that characteristic of AOBs, SKOV3 cells were incubated with fluorescent AOBs (25 μg ml^{-1}) for 2 h. After washing, cells were monitored for five days. During that time period, cells were sampled for analysis by confocal microscopy. Figure 7(b) shows that the fluorescent images in the cells decayed with time. As time elapsed, large fluorescent spots increasingly appeared, indicating the coalescence of unstable AOBs. After five days, the fluorescent signals were only marginally detected. Those findings imply that the hydrophobic dye is released from AOBs and decomposes within the cells.

Furthermore, the cumulative dye release profiles of AOBs *in vitro* were characterized. As shown in figure 7(c), the burst release was prominent at both pH values for the first 6 h. It was greater than 95% at pH 6.5 and 70% at pH 7.5. After this burst release, a constant and slow dye release was obtained until the end of the experiment. This gives a typical profile of the sustained and prolonged drug release, and the results are consistent with the common behavior reported for many drug delivery systems [32–34].

3.6. In vitro cytotoxicity of dye-loaded AOBs against tumor cells

The biocompatibility of AOBs loaded with the dye (50 mg ml^{-1}) with cells was evaluated along the time course. As depicted in figure 8, after three days cell viability of MDA-MB-231 was 76%, 97%, and 93% in cells exposed to the dye (oil/dye), Ole-based AOBs, and ZH2-based AOBs, respectively. It implies that the slight toxicity of the dye and encapsulation of the dye into AOBs readily shields from its toxicity. Meanwhile, cell viability of SKOV3 reached 70%, 90%, and 74% in cells treated with the dye, Ole-based AOBs, and ZH2-based AOBs, respectively. Nevertheless, no significant cytotoxicity was observed after three days of various treatments. The result indicates that AOBs are generally not cytotoxic.

4. Conclusion

Many anti-tumor drugs are highly toxic as well as hydrophobic and, therefore, frequently lead to serious side effects. The general solution to this problem relies on the use of a nanosized drug carrier system. Liposomes and micelles both assume a closed colloidal structure. The former contains a central aqueous space encircled by an outer lipid bilayer whereas the latter has a hydrophobic core surrounded by a hydrophilic shell. A variety of anti-cancer drugs have been encapsulated by these lipid-based systems [7, 35, 36]. AOBs have a similar structure but comprise an Ole-embedded lipid monolayer that surrounds a central oil space. As illustrated in this study, AOBs could be made functional simply by manipulation of Ole. Meanwhile, two extruded peptide arms of Ole confer on AOBs a negative surface charge [16], which would prevent undesired interaction with non-target cells [37]. Bringing the protein, plant oil, and PLs together, AOBs self-assemble in a facile and reproducible way. This leads to the controllability of their size in response to the oil/protein ratio and pH, allowing AOBs to be created on a nanoscale. The central oil space of AOBs facilitates the entrapment of hydrophobic agents. In particular, AOBs are non-cytotoxic, and they remain stable at the permissive conditions and are sensitive to acidic pH. All these features make AOBs very appealing as delivery carriers. The usefulness of AOBs for targeted delivery of hydrophobic drugs is currently under investigation in our laboratory.

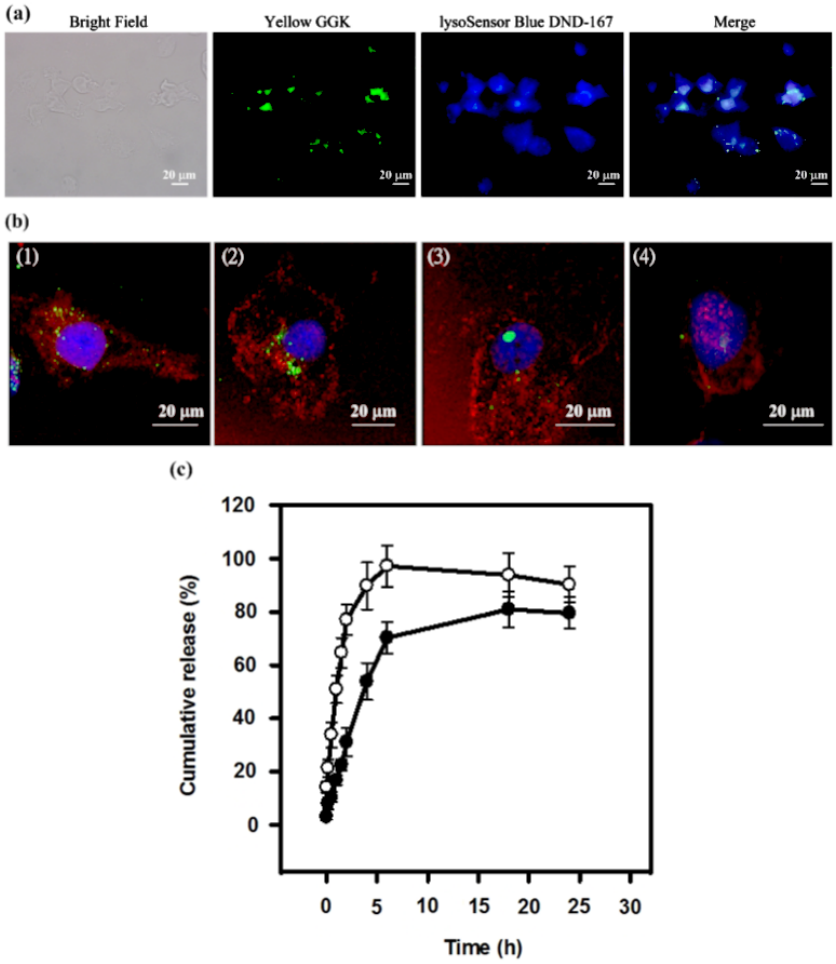

Figure 7. Release of the fluorescence dye carried by AOBs. (a) SKOV3 cells were cultured overnight on a Lab-Tek chamber slide system (Nalge Nunc International). Following co-incubation with fluorescent ZH2-based AOBs for 2 h, cells were washed with PBS and examined for green fluorescence by confocal microscopy. Subsequently, 1 μM LysoSensor blue DND-167 (Invitrogen) in DMEM without phenol red was added for 1 h. After washing with PBS, cell lysosomes were stained blue for observation by confocal microscopy. The panel shown on the right represents the overlay of the two images. (b) Co-incubation of SKOV3 cells with fluorescent ZH2-displayed AOBs was carried out in a similar way. The fate of internalized AOBs in the cells was tracked along the time course. Cells were taken for analysis by confocal microscopy on (1) day 0, (2) day 1, (3) day 3, and (5) day 5. (c) Loaded with 6.25 μg ml^{-1} dye, AOBs were processed for dye release at pH 6.5 (○) or pH 7.5 (●) and 37 °C for 24 h. The experiment was conducted in triplicate.

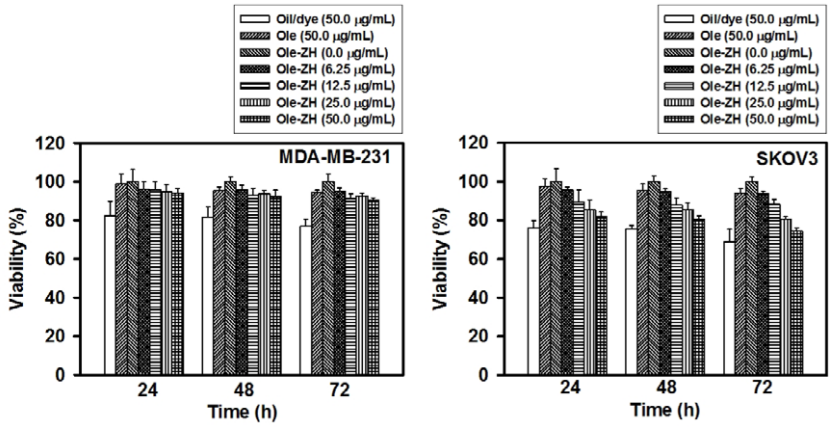

Figure 8. Cytotoxicity assay. Loaded with various concentrations of the hydrophobic dye, AOBs composed of Ole-ZH2 or Ole were used for the assay as described. Free dye mixed with sesame oil (oil/dye) was employed as a control. Co-incubation of (a) MDA-MB-231 ($n = 3$) and (b) SKOV3 ($n = 3$) with oil/dye or dye-loaded AOBs (Ole or Ole-ZH) was carried out for 24, 48 and 72 h. Cell viability was determined by the cell-counting kit.

Acknowledgments

We gratefully thank the Instrument Center of R&D Office at China Medical University for technical assistance and Mr Jeffrey Conrad for a critical review of this manuscript. This study was co-supported by the National Science Council of Taiwan (Grant no. NSC 97-2313-B-039-005), China Medical University (Grant no. CMU 98-C-11, CMU98-N2-22) and Feng Chia University (Grant no. 08G27501).

References

[1] Garrett J T, Rawale S, Allen S D, Phillips G, Forni G, Morris J C and Kaumaya P T 2007 Novel engineered trastuzumab conformational epitopes demonstrate *in vitro* and *in vivo* antitumor properties against HER-2/*neu* *J. Immunol.* **178** 7120–31

[2] Yip Y L and Ward R L 2002 Anti-ErbB-2 monoclonal antibodies and ErbB-2-directed vaccines *Cancer Immunol. Immunother.* **50** 569–87

[3] Qiu X Q, Wang H, Cai B, Wang L L and Yue S T 2007 Small antibody mimetics comprising two complementarity-determining regions and a framework region for tumor targeting *Nat. Biotechnol.* **25** 921–9

[4] Lipinski C A, Lombardo F, Dominy B W and Feeney P J 2000 Experimental and computational approaches to estimate solubility and permeability in drug discovery and development settings *Adv. Drug Deliv. Rev.* **46** 3–36

[5] Fernandez A M *et al* 2001 N-succinyl-(β-alanyl-l-leucyl-l-alanyl-l-leucyl)doxorubicin: an extracellularly tumor-activated prodrug devoid of intravenous acute toxicity *J. Med. Chem.* **44** 3750–3

[6] Andresena T L, Jensenb S S and Jørgensen K 2005 Advanced strategies in liposomal cancer therapy: problems and prospects of active and tumor specific drug release *Prog. Lipid Res.* **44** 68–97

[7] Zhang L, Chan J M, Gu F X, Rhee J W, Wang A Z, Radovic-Moreno A F, Alexis F, Langer R and Farokhzad O C 2008 Self-assembled lipid-polymer hybrid nanoparticles: a robust drug delivery platform *ACS Nano* **2** 1696–702

[8] Torchilin V P 2005 Lipid-core micelles for targeted drug delivery *Curr. Drug Deliv.* **2** 319–27

[9] Cohen S N and Bernstein H 1996 *Microparticulate Systems for the Delivery of Proteins and Vaccines* (New York: Dekker)

[10] Torchilin V P 2007 Micellar nanocarrier: pharmaceutical perspectives *Pharm. Res.* **24** 1–16

[11] Huang A H 1996 Oleosins and oil bodies in seeds and other organs *Plant Physiol.* **110** 1055–61

[12] Napier J A, Stobart A K and Shewry P R 1996 The structure and biogenesis of plant oil bodies: the role of the ER membrane and the oleosin class of proteins *Plant Mol. Biol.* **31** 945–56

[13] Frandsen G I, Mundy J and Tzen J T C 2001 Oil bodies and their associated proteins, caleosin and oleosin *Physiol. Plant* **112** 301–7

[14] Tai S S K, Chen M C M, Peng C C and Tzen J T C 2002 Gene family of oleosin isoforms in sesame seed oil bodies *Biosci. Biotechnol. Biochem.* **66** 2146–53

[15] Tzen J T C, Lie G C and Huang A H 1992 Characterization of the charged components and their topology on the surface of plant seed oil bodies *J. Biol. Chem.* **267** 15626–34

[16] Tzen J T C and Huang A H 1992 Surface structure and properties of plant seed oil bodies *J. Cell Biol.* **117** 327–35

[17] Tzen J T C, Chuang R L, Chen J C and Wu L S 1998 Coexistence of both oleosin isoforms on the surface of seed oil bodies and their individual stabilization to the organelles *J. Biochem.* **123** 318–23

[18] Peng C C, Lin I P, Lin C K and Tzen J T C 2003 Size and stability of reconstituted sesame oil bodies *Biotechnol. Prog.* **19** 1623–6

[19] Peng C C, Chen J C F, Shyu D J H, Chen M J and Tzen J T C 2004 A system for purification of recombinant proteins in *Escherichia coli* via artificial oil bodies constituted with their oleosin-fused polypeptides *J. Biotechnol.* **111** 51–7

[20] Chiang C J, Chen H C, Chao Y P and Tzen J T C 2005 Efficient system of artificial oil bodies for functional expression and purification of recombinant nattokinase in *Escherichia coli* *J. Agric. Food Chem.* **53** 4799–804

[21] Hou R C, Lin M Y, Wang M M and Tzen J T C 2003 Increase of viability of entrapped cells of *Lactobacillus delbrueckii* ssp.*bulgaricus* in artificial sesame oil emulsions *J. Dairy Sci.* **86** 424–8

[22] Chiang C J, Chen H C, Kuo H F, Chao Y P and Tzen J T C 2006 A simple and effective method to prepare immobilized enzymes using artificial oil bodies *Enzyme Microbiol. Technol.* **39** 1152–8

[23] Orlova A *et al* 2006 Tumor imaging using a picomolar affinity HER2 binding affibody molecule *Cancer Res.* **66** 4339–48

[24] Miller J H 1972 *Experiments in Molecular Genetics* (Cold Spring Harbor, NY: Cold Spring Harbor Laboratory Press)

[25] Chiang C J, Chen H C, Chao Y P and Tzen J T C 2007 One-step purification of insoluble hydantoinase overproduced in *Escherichia coli Protein Expr. Purif.* **52** 14–8

[26] Hung M C and Lau Y K 1999 Basic science of HER2/*neu*: a review *Sem. Oncol.* **26** 51–9

[27] Citri A and Yarden Y 2006 EGF-ERBB signalling: towards the systems level *Nat. Rev. Mol. Cell Biol.* **7** 505–16

[28] Steffen A C, Orlova A, Wikman M, Nilsson F Y, Ståhl S, Adams G P, Tolmachev V and Carlsson J 2006 Affibody-mediated tumour targeting of HER-2 expressing xenografts in mice *Eur. J. Nucl. Med. Mol. Imaging* **33** 631–8

[29] Alexis F *et al* 2008 HER-2-targeted nanoparticle–affibody bioconjugates for cancer therapy *ChemMedChem* **3** 1839–43

[30] Giri D K, Ali-Seyed M, Li L Y, Lee D F, Ling P, Bartholomeusz G, Wang S C and Hung M C 2005 Endosomal transport of ErbB-2: mechanism for nuclear entry of the cell surface receptor *Mol. Cell Biol.* **25** 11005–18

[31] Ohkuma S and Poole B 1978 Fluorescence probe measurement of the intralysosomal pH in living cells and the perturbation of pH by various agents *Proc. Natl Acad. Sci. USA* **75** 3327–31

[32] Kim G Y *et al* 2007 Resorbable polymer microchips releasing BCNU inhibit tumor growth in the rat 9L flank model *J. Control. Release* **123** 172–8

[33] Yang Z, Zhang Y, Markland P and Yang V C 2002 Poly(glutamic acid) poly(ethylene glycol) hydrogels prepared by photoinduced polymerization: synthesis, characterization, and preliminary release studies of protein drugs *J. Biomed. Mater. Res.* **62** 14–21

[34] Fung L K, Shin M, Tyler B, Brem H and Saltzman W M 1996 Chemotherapeutic drugs released from polymers: distribution of 1,3-bis(2-chloroethyl)-1-nitrosourea in the rat brain *Pharm. Res.* **13** 671–82

[35] Elbayoumi T A, Pabba S, Roby A and Torchilin V P 2007 Antinucleosome antibody-modified liposomes and lipid-core micelles for tumor-targeted delivery of therapeutic and diagnostic agents *J. Liposome Res.* **17** 1–14

[36] Shmeedaa H, Tzemacha D, Maka L and Gabizon A 2009 Her2-targeted pegylated liposomal doxorubicin: retention of target-specific binding and cytotoxicity after *in vivo* passage *J. Control. Release* **136** 155–60

[37] Suh W, Han S O, Yu L and Kim S W 2002 An angiogenic, endothelial-cell-targeted polymeric gene carrier *Mol. Ther.* **6** 664–72